Geophysical Prospecting

EAGE EUROPEAN ASSOCIATION OF GEOSCIENTISTS & ENGINEERS

*Geophysical Prospecting* doi: 10.1111/j.1365-2478.2010.00867.x

# Comparison of surface and borehole locations of induced seismicity

Leo Eisner[1]*, B. J. Hulsey[1], Peter Duncan[1], Dana Jurick[2], Heigl Werner[3] and William Keller[4]

[1]*Microseismic Inc., 1300 W Sam Houston Pkwy, Suite 200, Houston, TX 77042, USA,* [2]*Devon Energy Corporation, Devon Energy Tower, 1200 Smith Street, Houston, TX 77002-4313, USA,* [3]*Apache Corporation, 2000 Post Oak Boulevard, Suite 100, Houston, Texas 77056-4400, USA, and* [4]*Chesapeake Energy Corporation, PO Box 18496, Oklahoma City, OK 73154-0496, USA*

Received June 2009, revision accepted December 2009

## ABSTRACT

Monitoring of induced microseismic events has become an important tool in hydraulic fracture diagnostics and understanding fractured reservoirs in general. We compare microseismic event and their uncertainties using data sets obtained with surface and downhole arrays of receivers. We first model the uncertainties to understand the effect of different acquisition geometries on location accuracy. For a vertical array of receivers in a single monitoring borehole, we find that the largest part of the final location uncertainty is related to estimation of the backazimuth. This is followed by uncertainty in the vertical position and radial distance from the receivers. For surface monitoring, the largest uncertainty lies in the vertical position due to the use of only a single phase (usually P-wave) in the estimation of the event location. In surface monitoring results, lateral positions are estimated robustly and are not sensitive to the velocity model.

In this case study, we compare event location solutions from two catalogues of microseismic events; one from a downhole array and the second from a surface array of 1C geophone. Our results show that origin time can be reliably used to find matching events between the downhole and surface catalogues. The locations of the corresponding events display a systematic shift consistent with a poorly calibrated velocity model for downhole dataset. For this case study, locations derived from surface monitoring have less scatter in both vertical and horizontal directions.

**Key words:** Hydraulic fracturing, Locations, Microseismic monitoring, Uncertainty.

## INTRODUCTION

A microseismic event is generated at an unknown origin time and unknown location (so-called hypocentre). By observing the arrival times of the P- and S-waves of an event at a sufficiently large network of sensors, an estimate of the hypocenter location and origin time can be made through the process of trilateration. With restricted receiver distributions, such as receivers in a vertical monitoring borehole, additional information about the hypocenter has to be derived from particle polarization measurements (Pearson 1981; Phillips *et al.* 1989; Fischer *et al.* 2008). Using 3-component sensors, the polarization of the first event arrival, i.e., wavefront propagation direction, may be determined, giving an additional constraint on the direction the first arrival came from. However, particle polarization of a P- or S-wave is a local measurement at the sensor while arrival time is an integral measurement. Thus, source parameters inverted from particle polarization are more affected by local heterogeneities near the sensors than those obtained from an inversion of arrival times.

* E-mail: leisner@microseismic.com

This is the result of using P- or S-wave rays to locate microseismicity as the rays are only high-frequency approximation to trajectories along which seismic energy propagates, or in other words they are solutions of a high-frequency asymptotic series (Červený 2001). Traveltimes are evaluated as solutions of the first-order term, eikonal equation, i.e., the most stable part of the high-frequency approximation. However the particle polarization results from the second-order term, the transport equation, which is only a higher order correction on the eikonal equation.

It is therefore desirable to have spatially distributed receivers (whether at the surface or in the subsurface). Microseismic events by definition have weak signals and suffer from further attenuation in shallow layers of sedimentary basins. For example, surface recordings of S-waves have typically lower signal-to-noise ratio than P-waves due to attenuation (Kolínský *et al.* 2009) despite their significantly better signal-to-noise ratio in the vicinity of the source. Using multiple phases (such as P- and S-waves) requires multiple velocity models in the location algorithm resulting in additional sources of uncertainty. Therefore, published case studies (e.g., Lakings *et al.* 2005) with spatially distributed receivers rely on single phase (P-wave) locations. Locations derived from only single phase however suffer from a trade-off between origin time and hypocentral position, as will be discussed later.

Eisner *et al.* (2009) numerically simulated uncertainties for frequently used receiver geometries in both borehole and surface acquisition in order to compare both approaches. In the present paper, we give a detailed description of their probabilistic methodology and further results calculating the likely error in hypocenter estimates. We discuss how these errors are affected by the location of the sensor array, frequency content of the data and picking accuracy. We focus on two scenarios that are commonly applied in practice: a 2D grid of receivers on the earth's surface and a linear array of receivers in a single vertical borehole. Eisner *et al.* (2009) also presents a limited study of the effect of errors in the velocity model assuming a homogeneous medium, recognizing that heterogeneity may have as profound an effect on location accuracy as receiver distribution (e.g., Maxwell 2009).

Finally, we describe a case study where microseismicity was induced by hydraulic fracturing and monitored from both a vertical borehole and the surface. Two catalogues of microseismic events are systematically analysed and matched to identify the same events in both data sets. Most of the discrepancies in event locations obtained from the two arrays are consistent with the previously discussed sources of uncertainties.

## METHOD

In order to compare the uncertainties of different types of location techniques (i.e., arrival times with azimuthal measurements and single phase arrival times only) we calculate probability density functions of hypocenters derived from synthetic (perfect) measurements assuming their errors are Gaussian. Deviations from this assumption will be discussed in a later section. We shall assume that azimuths and arrival times have Gaussian distributions around the true values that we obtain from forward modelling. The Gaussian distribution allows us to compare different kinds of measurements (arrival times and azimuths) and different techniques of hypocenter locations (single arrival times versus relative P- to S-wave arrival times) as each measurement is normalized by its standard deviation. Thus we model the probability density of a hypocentre due to a single receiver and an uncertain measurement is

$$p(x) = \frac{1}{\sigma\sqrt{2\pi}} e^{-(x-x_m-x_0)^2/2\sigma^2}, \tag{1}$$

where $x$ is the measured variable (P- or S-wave arrival time or backazimuth), $x_m$ is the model derived value (P- or S-wave traveltime or backazimuth derived from velocity model and location), $t_0$ is origin time for arrival times and zero for azimuthal measurement and $\sigma$ is the standard deviation of the measured variable $x$. The standard deviation $\sigma$ can be estimated from a distribution of the observed arrival times, a fit to the traveltimes for a location and velocity model, or from RMS deviation between modelled and measured azimuths.

Now assuming that each sensor and the measured quantities are mutually independent we can combine the probability density functions by multiplying the individual probabilities as

$$p(t_P, t_S, A) = N e^{-\sum_R (t_P - t_{mP} - t_0)^2/2\sigma_P^2} e^{-\sum_R (t_S - t_{mS} - t_0)^2/2\sigma_S^2} e^{-\sum_R (A - A_m)^2/2\sigma_A^2}, \tag{2}$$

where $t_P$, $t_S$ and $A$ are measured arrival times of P- and S-waves and measured backazimuth, respectively. $t_{mP}$, $t_{mS}$ and $A_m$ are computed values of P- and S-wave traveltimes and azimuth (e.g., computed by a ray method), $t_0$ is the origin time and $\sigma_P$, $\sigma_S$ and $\sigma_A$ are the standard deviations of the measured P- and S-wave arrival times and azimuth, respectively. Summations in the exponents of equation (2) are carried out over all receivers where either P- or S- or azimuthal measurements are made. The normalization constant $N$ ensures that the integral of the above expression over all possible locations is equal to one.

In this study, we evaluate equation (2) for all possible origin times $t_0$ at each potential location in a grid search fashion (i.e.,

we search over all possible origin times and locations). For each location point the final probability is the maximum over all possible origin times. This formulation allows for arbitrary distribution of receivers and arbitrary velocity model. If more phases, such as split S-waves, are used one can simply add corresponding exponential terms in equation (2). For example, in the case of a vertical component measured at the surface, only the exponential term with P-waves is used (the other two are set to one). The uncertainties ($\sigma_P$, $\sigma_S$ and $\sigma_A$) reflect the quality of the data, the ability to fit the data with a given velocity model and the amount of seismic noise. In this way, data of different quality can be combined. For example, let us assume that the standard deviation of an arrival time is proportional to the peak frequency of the observed signal, then $\sigma_P$ of a signal with a peak frequency at 100 Hz (borehole) will have approximately 2.5-times smaller $\sigma_P$ than P-wave arrival with peak spectra at 40 Hz (surface). Hence location uncertainty will also be 2.5-times smaller.

We have assumed in equation (2) that measurements are mutually independent and Gaussian. In reality, most of the location techniques do not measure these values independently (e.g., Rutledge and Phillips 2003). For example, backazimuths are measured in time windows derived from picked arrival times. Another challenge arises from non-Gaussian distribution of the measurement errors, for example Bulant *et al.* (2007) showed that small errors in deviation surveys of the monitoring boreholes cause systematic biases in measured backazimuths. Arrival time picks can be biased by attenuation if picked on maximum amplitude or signal-to-noise ratio if picked on onset. Finally, velocity model errors are perhaps the most significant source of location biases in both surface and downhole monitoring, however accounting for such errors is very difficult as they are model dependent.

The mutual dependency and non-Gaussian distribution of measurements mean that the probability density function of equation (2) would have to be computed in an even more complicated fashion using covariances (Tarantola and Valette 1982). With the simplifying assumption of mutual independence, the above evaluation of probability density functions (equation (2)) is going to give the lower bound on uncertainties from various receiver configurations and data quality (frequency, velocity model) independent of a particular picking technique.

In the next part of this study we use computed traveltimes and azimuth for a chosen location as 'measured' traveltimes and azimuth, $t_{mP}$, $t_{mS}$ and $A$ in equation (2) and calculate joint probability densities of hypocenters for borehole and surface monitoring arrays in order to quantify uncertainties for a typical monitoring geometry. To compute the 'measured data' we used ray synthetic traveltimes and backazimuth in a homogeneous isotropic medium.

## LOCATIONS FROM A VERTICAL BOREHOLE ARRAY

Eisner *et al.* (2009) illustrated how arrival times of P- and S-waves from a single receiver only constrain the radial distance of the hypocenter from this receiver. All points on the surface of a sphere whose radius is equal to this distance are potential hypocenters. Multiple receivers in a monitoring borehole constrain multiple spheres; they intersect at the true location. The shorter the array is, the more concentric these spheres are and the less constrained the vertical position of the hypocenter is (for vertical borehole). The uncertainty in radial direction is determined from standard deviation in arrival times and their fit to the traveltimes of P- and S-waves. We have assumed the standard deviations in both P- and S-wave arrival time picks to be 1 ms ($\sigma_P = \sigma_S = 1$ ms) for downhole monitoring. This standard deviation in arrival times reflects several aspects of the data: frequency content of P- and S-waveforms, consistency of the arrival times and ability to fit the arrival times with traveltimes determined from a velocity model. While most of the service companies offer downhole microseismic monitoring with sampling of 0.25 ms or better, the sample interval alone does not necessarily control the standard deviation of the arrival times. While it is not possible to say which factor dominates as the factors vary from data set to data set, we can assume that 1 ms is a lower bound of the standard deviation $\sigma$ from a published case study with high quality data: Rutledge and Phillips (2003) located hundreds of microseismic events with rms time residuals up to 5 ms and a median RMS (root-mean-square) 1.3 ms, hence our value of 1 ms in lower bound. While some may argue that 'station statics' allow an even higher accuracy, we would like to remind a careful reader that such 'station statics' are not constant, especially in downhole acquisition where ray trajectories change rapidly from event to event as rays travel parallel to the sedimentary bedding. In other words, nearly horizontal travelling rays may encounter a very complicated travelpath in vertically stratified sedimentary media. Such horizontal propagation or near-surface conditions can be to some extent modelled with allowing different standard deviations for different receivers.

Figure 1 shows 1D marginal probability densities for $\sigma_P = \sigma_S = 1$ms and a backazimuth standard deviation $\sigma_A = 10^\circ$. As 'data' we have used exact traveltimes computed in a homogeneous isotropic medium and the exact

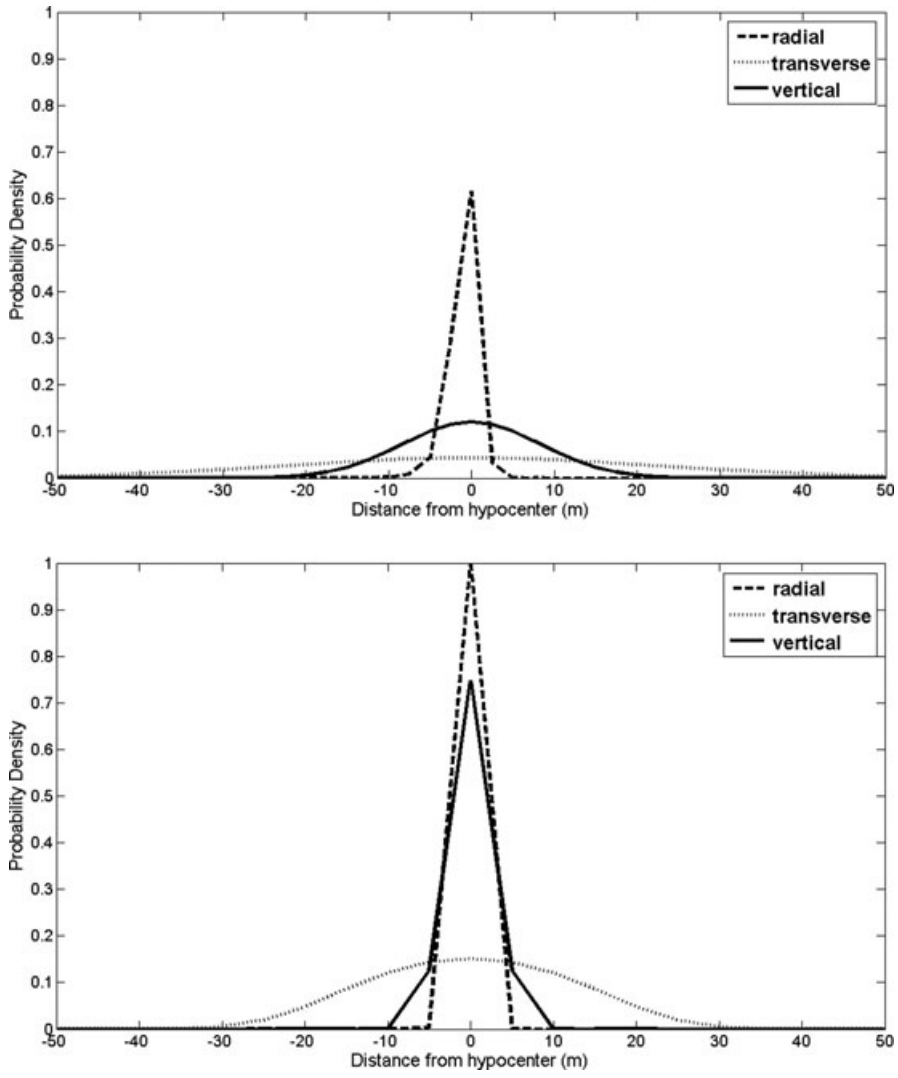


**Figure 1** Marginal probability density functions of a hypocenter located at the central depth of a monitoring array at a distance of 300 m. Both panels represent vertical monitoring arrays at 300 m horizontal distance from hypocenter, top panel represents 5 receivers spanning 120 m, bottom panel represents 11 receivers spanning 300 m. We used a standard deviation of 1 ms for arrival times and 10° for the backazimuth.

backazimuths computed in homogeneous isotropic medium. The standard deviation of 10° is based on Eisner, Fischer and Rutledge (2008) who showed that, for a well understood data set, standard deviations of P-wave derived backazimuths are approximately 29° and more than 10° in backazimuth measurement between S-waves. Note that a backazimuth can be measured to a greater precision for some strong events on a single receiver. However, Eisner, Fischer and Rutledge (2008) showed that the consistency of these azimuthal measurements across the borehole array can be poor and there is a systematic discrepancy between P- and S-wave derived backazimuths.

Note that the transverse (azimuthal) uncertainty also shown in Fig. 1 dominates the location inaccuracy; even in the ideal case of the hypocenter being at the centre depth of the downhole array. Thus we may conclude that the radial coordinate of the location obtained from a vertical borehole array is the best constrained coordinate, next is most likely the vertical coordiante (although this depends on the relative position of the event and monitoring array) and the worst constrained coordinate is the transverse (azimuthal) one. We calculated standard deviations and obtained 2 m in the radial direction, 23 m in the transverse (azimuthal) direction and 8 m in the vertical direction for a receiver array spanning 120 m. A receiver array spanning 300 m has radial and vertical deviations reduced to 1.5 and 4 m, respectively but the transverse deviation of 20 m remains approximately the same. Figure 1

illustrates that the shorter the array length the larger depth uncertainty and that the depth uncertainty is usually larger than the radial uncertainty. Note that the above uncertainties are relative to the correct velocity model and including velocity model uncertainty may significantly extend the location uncertainty.

## LOCATIONS FROM SURFACE ARRAYS

Surface locations are derived from large arrays distributed in a 2D grid. In this synthetic example, we shall assume that all arrival times are determined on 121 receivers organized in an 11 by 11 rectangular grid with 600 m receiver spacing. The probability density of a hypocentre is mainly constrained by the offset of the array from the epicentre. We consider locating events occurring at a 3000 m depth monitored from a 6000 by 6000 m array. The shortest offset for an event with an epicentre at the centre of the array is 3000 m.

Figure 2 shows the uncertainty of an event located with a surface array assuming a standard deviation of 4 ms for arrival times, which is estimated from an average misfit between synthetic traveltimes and observed arrival times in multiple data sets with strong events where visible P-wave arrivals were measurable and ranged from 2.7–3.4 ms across hundreds of receivers. Furthermore, the P-wave velocity model is usually better constrained (from active surface seismic) and receiver statics do not rapidly change with the locations of microseismic events, as the receiver array is much larger than

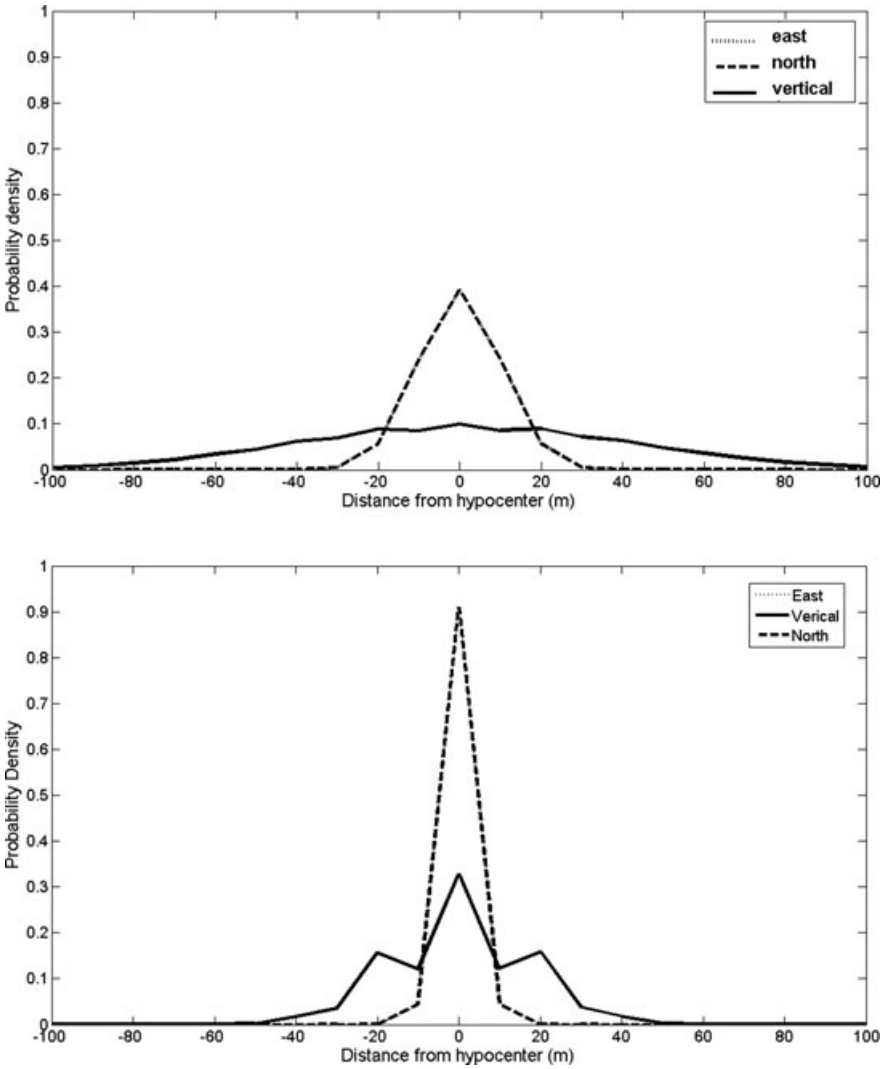


**Figure 2** Marginal probability density functions of a hypocenter located 3000 m below the centre. We used standard deviation of 10 (top plot) and 4 ms (bottom plot) for arrival times of P-waves. An array of 121 receivers at the surface with offset to depth ratio approximately 1:1. The solid and dotted lines overlay as these probabilities are exactly the same.

distances between located events. Note that the horizontal position is relatively well constrained (standard deviations are 3 m in both radial and transverse directions, rather than X- and Y-coordinates) while the vertical position suffers from the trade-off between origin time and depth (standard deviation is 17 m). The uncertainties are relative to the correct velocity model and including velocity model uncertainty may significantly increase the location uncertainty as shown by Eisner *et al.* (2009).

## CASE STUDY

Event locations from surface and downhole arrays were compared on a field data set recorded during a hydraulic fracture stimulation performed in a horizontal treatment well at a depth of approximately 2200 m. Five independent stages of slurry with a proppant were injected into a shale formation. We will compare only the best signal-to-noise ratio events from the last of the five stages. This stimulation was monitored with a linear downhole and star-shaped surface array (Fracstar®). The surface array detected and located approximately 99 events using a matched filter (Eisner *et al.* 2008; Hulsey *et al.* 2009) applied to the stacking of 773 surface receivers. The matched filter technique provides highly accurate locations relative to a master event location reducing dependency on the velocity model. The downhole monitoring of 17 3C geophone arrays detected and directly located 171 events and the monitoring geometries are illustrated in Fig. 3 (the downhole array spanned approximately 100 m vertically).

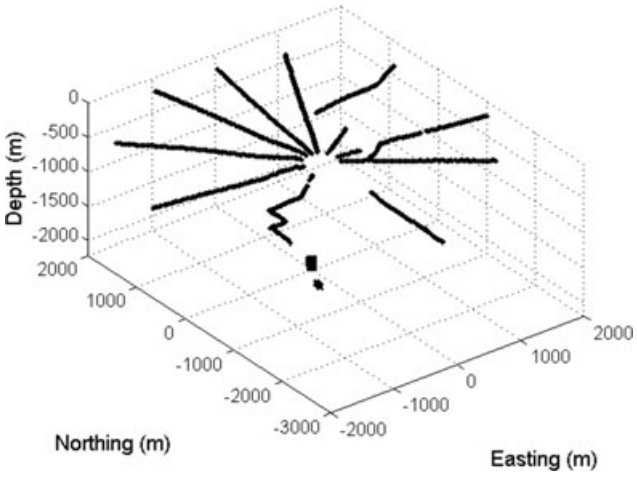


**Figure 3** 3D view of the monitoring geometry: diamods represent vertical component geophones at surface, squares represent borehole monitoring 3C geophones and crosses represent the perforations intervals of stage 5.

Both techniques used different velocity models. Map views and timing of both surface and downhole located events are shown in Fig. 4. This figure illustrates a typical problem in the interpretation of joint data sets where the induced microseismic events are monitored with surface and downhole geophones. Downhole locations in this data set suggest two offset fractures striking at an approximate azimuth of 70° while events located with surface monitoring array could be interpreted as a single fracture zone with an azimuth of approximately 80°. Both data sets show more events in the western part of the fracture during the first hour of stimulation and

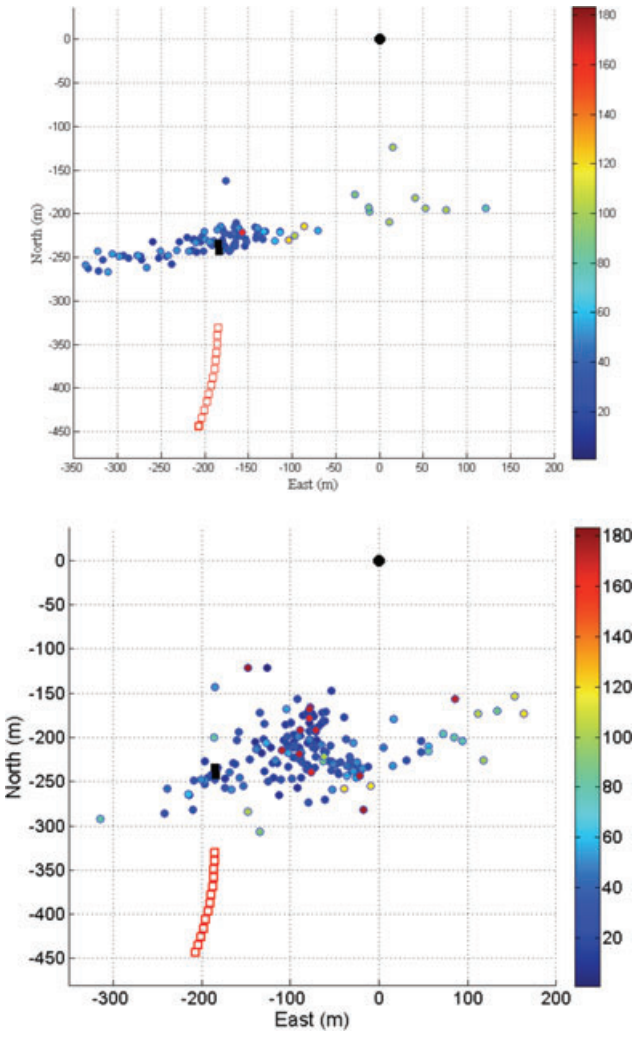


**Figure 4** Map views of microseismicity located from surface (top) and downhole (bottom) monitoring arrays. Fracstar located 99 events, while downhole array located 171 events. Origin times are represented by colour coding. Downhole monitoring array is represented as a black circle on the north-east part of each plot. Perforation interval of stages 5 and 4 are represented by red and black squares, respectively.

both seem to originate from perforation interval number 4 instead of 5. While the locations of the surface data set were determined by the authors of this article, downhole locations were only provided by the operator and we were unable to verify them with our own inversion for the purpose of this study. We obtained magnitudes of the 10 strongest downhole events; the remaining 161 downhole events were provided only with locations and origin times. Furthermore, all origin times of downhole events were rounded to the nearest second. While this is not ideal for a scientific test, it is the best data set we have for publication.

As discussed and demonstrated in the modelling section of this study, the most accurate information on microseismic events can be derived from an inversion of arrival times rather than local parameters such as particle polarization, orientation or amplitude. In this case study it can be illustrated in the following way: origin time, which is derived from arrival times has, an uncertainty of 0.5 second, at worst, because the origin times of the downhole data set were rounded off to the nearest second. Induced seismicity occurs for approximately 3 hours or 10 800 seconds or approximately 3 hours. However, locations derived from polarization measurements have standard deviation of approximately tens of metres, while the transverse distance over which they occur (fracture length perpendicular to the monitoring array) is approximately 300–400 m. Thus the uncertainty in origin time is only 0.5/10800 ~0.004% of the space in which the event is likely to occur while uncertainty in location is at least 10/400 ~2.5% of this space. Similarly, we can show that magnitude or source mechanism inversions are even more uncertain relative to the space in which we wish to match the two catalogues. Thus to match two catalogues of (micro-) earthquakes we propose to start by matching origin times and use locations only to verify the match.

However, the absolute timing of both systems was not certain and we did not find a reasonable match with the times provided. Therefore we decided to shift all origin times of downhole located events by 3 minutes and 20 seconds to match the origin times between the largest downhole and the largest surface event. This shift provided matching origin times between surface events and the remaining nine downhole strongest events within 0.5 s as illustrated in Fig. 5. The timing match between two catalogues is significant as the likelihood that this agreement is random coincidence over 3 hours is very small. For example, let us assume we have approximately 100 surface origin times distributed randomly in 180 minutes: matching 1 downhole origin time by 0.5 s has a probability of $100 \times 1/180 \times 60 \sim 1/100$. Finding 9 matches within this interval by pure coincidence is $10^{-18}$ times as likely. Unfortunately, relative sizes of the seismic moments between the two data sets do not agree as shown in Fig. 5. As discussed previously seismic moments are less reliably inverted than origin times and we shall discuss this issue later.

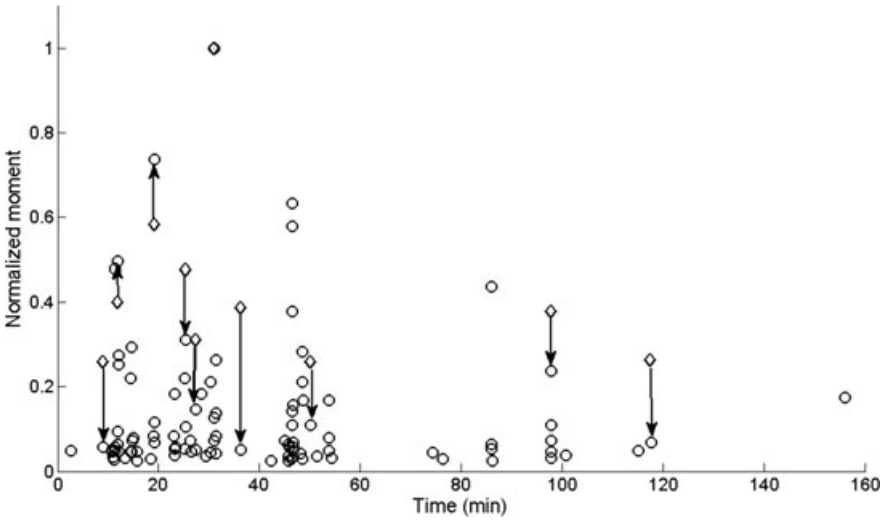


**Figure 5** Relative seismic moment versus origin time for surface (black circles) and top ten downhole (black diamonds) events. The seismic moments of the largest event from surface and the largest event from downhole were scaled to 1 and their relative origin times adjusted to match. Corresponding matches of the remaining 9 events are represented by the black arrows. Horizontal axis shows time in minutes since beginning of the fracturing.

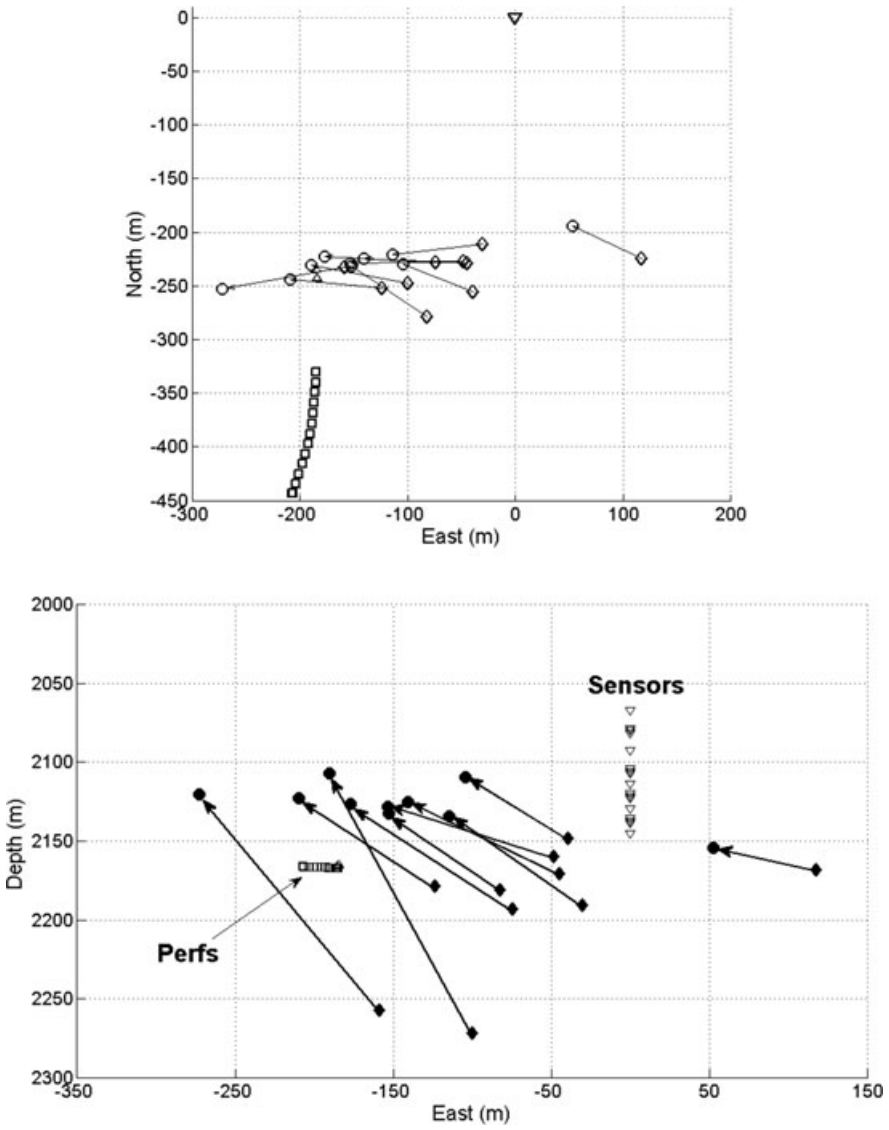


**Figure 6** Map view (top) and east-west vertical cross-section (bottom) of the ten strongest downhole and corresponding surface hypocenters. Open diamonds represent downhole locations and open circles represent corresponding surface events found by origin time matching shown in Fig. 5. The origin time match is represented by a black arrow. Black squares and triangles represent perforation interval of the 5$^{th}$ and 4$^{th}$ stages, upside-down triangles represent 17 borehole geophones used for the downhole monitoring.

The match between surface and downhole events derived from origin times can be verified by careful analysis of locations of these events. Figure 6 shows a map view and a vertical cross-section of the ten matched events. The surface and downhole located events appear to be relatively shifted but this shift appears to be nearly constant for all events; the most western event from downhole locations is matched by origin time to the most western event in surface location and so on. This is actually a significant observation because locations and origin times are nearly independent in these data sets (definitely with 0.5 s accuracy on origin times) and if the match of origin times shown in Fig. 5 was just random coincidence, the shift between corresponding locations would be random too. The surface locations appear to be aligned along 80° azimuth (Fig. 4) while downhole locations appear to form a slightly dispersed cloud in east-west direction. There is an approximately 100 m westward shift from downhole to surface locations. In the depth cross-section, the surface locations appear to span

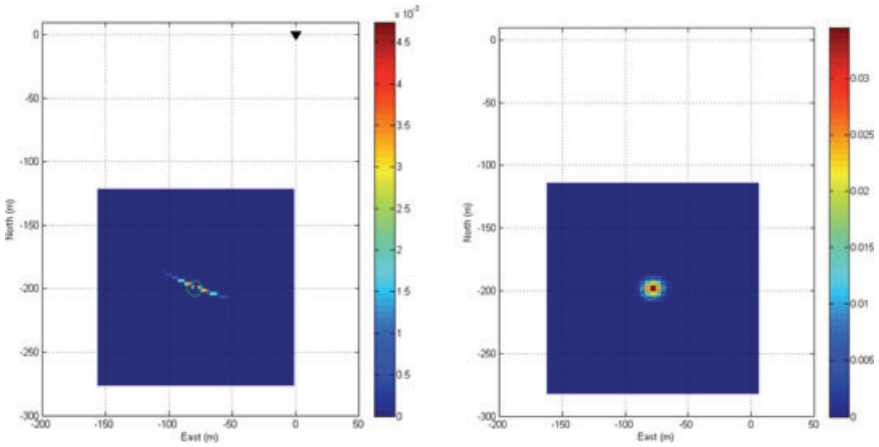


**Figure 7** Map views of a probability density function for a hypothetical microseismic event located at −80 m east and −200 m north coordinates from a vertical borehole array at 0,0 (left plot) and surface array (right plot). The vertical borehole array is represented by black triangles in the north-east corner of the left plot.

approximately 50 m while downhole locations are spanning approximately 120 m. Note that this figure represents the largest downhole events with the best signal-to-noise ratio. While we are not able to determine which set of locations is right, we are confident matched microseismic events mapped by both downhole and surface monitoring were caused by the same seismic event in the subsurface.

## DISCUSSION

The difference between surface and downhole locations shown in Fig. 6 may be due to several causes. The obvious 100 m western shift between these two data sets can be explained by adjusting the velocity model for downhole locations and rotation of the monitoring array (see Bulant *et al.* 2007). It is common practice to adjust downhole velocity models using early induced events in the vicinity of perforation intervals (it is justified by anisotropic velocities), however, we do not know if the downhole locations were calculated in this way. Surface locations are unlikely to be shifted in the horizontal plane as perforations of both the third and fifth stage were located within 20 m from their assumed positions (calculated from deviation surveys).

Surface monitoring located the first events approximately 100 m west of the perforation interval of stage 4 (note that this study analysed stimulation of injection interval 5 and stage 4 was already stimulated), while downhole monitoring located the corresponding first events in very close vicinity of the perforation interval of stage 4. Such an adjustment would also explain the difference in azimuths of Fig. 4, as the adjusted downhole model would shift eastern events towards the northerly monitoring borehole. Strong lateral heterogeneity is an unlikely cause of the location discrepancies as the surface locations are calculated with a relative location algorithm (removing effects of near-surface heterogeneities) and downhole locations are calculated in relatively flat sedimentary layers. As shown by probability density modelling, the surface locations do not seem to have any particular bias in horizontal coordinates. Thus it is unlikely that the difference of horizontal trends in Fig. 6 is caused by surface errors (80° azimuth surface versus east-west downhole trend). Also note that part of the downhole scatter appears to be along the azimuthal (transverse) direction from the monitoring borehole. To illustrate this point, Fig. 7 shows probability density function for surface and downhole geometry of this case study assuming homogeneous isotropic medium and exact picks with standard deviation of 1 ms and azimuthal deviation of 10°. The monitoring geometry causes the location uncertainty to be elongated in NW-SE direction, consistent with observed trends in downhole locations of the real events.

Perhaps the most surprising difference between the located events is shown in the vertical cross-section (Fig. 6). As discussed in the first section of this paper, one would expect the surface locations to have larger vertical scatter. All 99 surface locations seem to be consistently located to a depth interval spanning approximately 70 m while downhole locations seem to form two layers about 120 m apart in the vertical direction. It is unclear to us why surface locations would show a bias toward a particular depth. However, it is possible that the downhole model consisted of two fast layers that might

cause the locations to split between two layers and force most of the downhole locations to locate deeper than surface locations. The velocity model used in the surface method was again calibrated by locating the perforation shots of stage 3 and 5 within 20 m from their assumed depth.

This location bias due to horizontal layering is not addressed in the first part of this study, although it can be addressed for a particular model with the same proposed methodology. In fact, real reservoirs are neither homogeneous nor isotropic. The net effect is that rays are bent by heterogeneities and may not have a linear particle polarization (e.g., anisotropy, multipathing, local heterogeneities, near borehole effects, surface statics, etc.). In practice however, the particle polarization is reasonably stable within the azimuthal

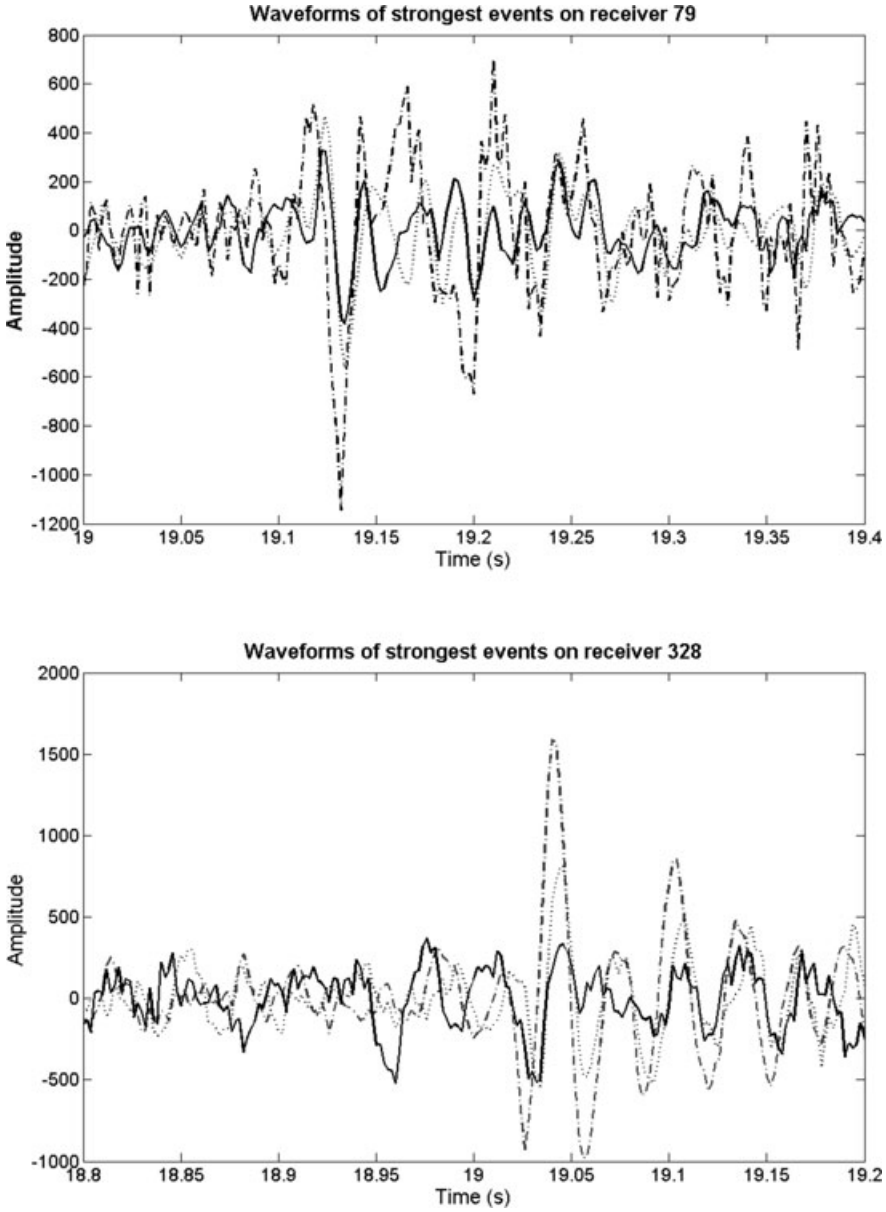


**Figure 8** Particle velocity of three microseismic events matched to the three largest (by seismic moment) downhole events. Top plot represents particle motion in the southern part of the array as shown in Fig. 3 while the lower plot shows particle velocities in the northern part of the array. Dash-dot lines represent particle velocities due to the largest event in downhole monitoring, solid line represents particle velocities due to the second largest event and dotted line represents the third largest event in the downhole data set.

standard deviation, as sedimentary basins are approximately horizontally layered. Thus we may conclude that the uncertainty estimates for borehole monitoring shown in Fig. 1 are a lower bound and this was also confirmed by the comparison in the case study. This conclusion is also supported by recently published studies (Maxwell 2009; Zimmer 2009) that take the 1D heterogeneity into account and found large radial and vertical errors (exceeding 100 m in realistic models). Our case study shows that surface and downhole microseismic monitoring have a similar order of uncertainty in the vertical direction, indicating that surface locations standard deviation of 4 ms is more representative than 10 ms. However, the actual shape of the location probability density function is dependent on the relative depth of a hypocenter relative to the centre of the downhole array and may actually introduce significant artefacts to the located hypocenters. Surface monitoring is more sensitive to an accurate velocity model for its vertical position but has the advantage that the needed vertical velocities can be obtained from surface seismic and perforation shots. The horizontal positions of the located microseismic events do not seem to be significantly affected for surface monitoring.

Finally, let us discuss the discrepancy between relative sizes of seismic moments of downhole and surface events (see Fig. 5). We have investigated recorded waveforms of the three surface seismic events corresponding to the three strongest downhole events. We have found that two of these events have signal higher than noise on a majority of the geophones and we show an overlay of the vertical particle velocities for two receivers in Fig. 8. Note that while particle velocity of the strongest event has the largest P-wave amplitude on both receivers (dash-dot line), the event with the second largest seismic moment (solid line) has actually smaller P-wave amplitudes than the event with the third largest moment (dotted line). While relative amplitudes at individual receivers may vary, this order is representative of the 600+ receivers and results from very similar source mechanisms also observed in downhole monitoring (e.g., Eisner, Fischer and Le Galvez 2006). Further analysis of magnitude inversion is required to make a more definite conclusion.

## CONCLUSIONS

We have formulated maximum likelihood location theory suitable for both downhole and surface monitoring of induced seismicity. This theory allowed us to compare downhole and surface location uncertainties in a consistent manner and we have shown that for commonly used distribution of receivers both monitoring techniques have similar uncertainties in a homogeneous isotropic medium. Case study comparison of downhole and surface locations confirmed that both techniques have similar uncertainties relative to a velocity model. However, locations of microseismic events from downhole monitoring are consistent with larger scatter in vertical direction and systematic shift relative to the monitoring array.

## ACKNOWLEDGEMENTS

The authors are grateful to Devon Energy for the release of this data set. The contribution from Mike Thornton was essential to this paper.

## REFERENCES

Bulant P., Eisner L., Pšenčík I. and Le Calvez J. 2007. Importance of borehole deviation surveys for monitoring of hydraulic fracturing treatments. *Geophysical Prospecting* **55**, 891–899.

Červený V. 2001. *Seismic Ray Theory*. Cambridge University Press.

Eisner L., Abbott D., Barker W.B., Lakings J. and Thornton M.P. 2008. Noise suppression for detection and location of microseismic events using a matched filter. 78th SEG meeting, Las Vegas, Nevada, USA, Expanded Abstracts, 1431–1435.

Eisner L., Fischer T. and Le Calvez J. 2006. Detection of repeated hydraulic fracturing (out-of-zone growth) by microseismic monitoring. *The Leading Edge* **25**, 547–554.

Eisner L., Fischer T. and Rutledge J. 2008. Determination of S-wave backazimuth from a linear array of borehole receivers. *Geophysical Journal International* **176**, 31–39. doi:10.1111/j.1365-246X.2008.03939.x

Eisner L., Heigl W., Duncan P. and Keller W. 2009. Uncertainties in passive seismic monitoring. *The Leading Edge* **28**, 648–655.

Fischer T., Hainzl S., Eisner L., Shapiro S.A. and Le Calvez J. 2008. Microseismic signatures of hydraulic fracture growth in tight-sandstone-shale formation: Observation and modeling. *Journal of Geophysical Research* **113**, B02307.

Hulsey B.J., Eisner L., Thornton M.P. and Jurick D. 2009. Application of relative location technique from surface arrays to microseismicity induced by shale fracturing. 79th SEG meeting, Houston, Texas, USA, Expanded Abstracts.

Kolínský P., Eisner L., Grechka V., Jurick D. and Duncan P. 2009. Observation of shear-wave splitting from microseismicity induced by hydraulic fracturing – A non-VTI story. 71st EAGE meeting, Amsterdam, the Netherlands, Expanded Abstracts.

Lakings J.D., Duncan P.M., Neale C. and Theiner T. 2005. Surface based microseismic monitoring of a hydraulic fracture well stimulation in the Barnett shale. 75th SEG meeting, Houston, Texas, USA, Expanded Abstracts, 605–608.

Maxwell S. 2009. Microseismic location uncertainty. *CSEG Recorder* (April), 41–46.

Pearson C. 1981. The relationship between microseismicity and high pore pressures during hydraulic stimulations experiments in low permeability granitic rocks. *Journal of Geophysical Research* **86**, 7855–7864.

Phillips W.S., Fairbanks T.D., Rutledge J.T. and Anderson D.W. 1989. Induced microearthquake patterns and oil-producing fracture systems in the Austin chalk. *Tectonophysics* **289**, 153–169.

Rutledge J.T. and Phillips W.S. 2003. Hydraulic stimulation of natural fractures as revealed by induced microearthquakes, Carthage Cotton Valley gas field, east Texas. *Geophysics* **68**, 441–452.

Tarantola A. and Valette B. 1982. Inverse problems = quest for information. *Journal of Geophysics* **50**, 159–170.

Zimmer U., Bland H., Jing D., Warpinski N., Sen V. and Wolfe J. 2009. Accuracy of microseismic event locations recorded with single and distributed downhole sensor arrays. 79th SEG meeting, Houston, Texas, USA, Expanded Abstracts, 1519–1523.